Measure and Evaluate
MRgRT 3D Distortion
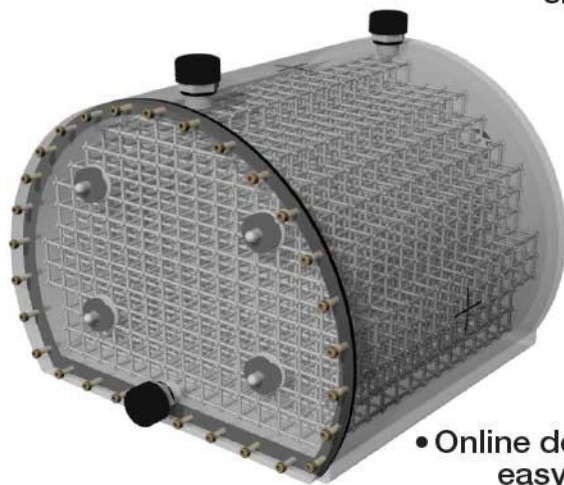
distortion check

CLOUD SOFTWARE FOR EVALUATION OF IMAGE DISTORTION

SCAN

UPLOAD IMAGES

REVIEW REPORTS & TREND ANALYSIS

EXPORT DICOM OVERLAYS TO TPS
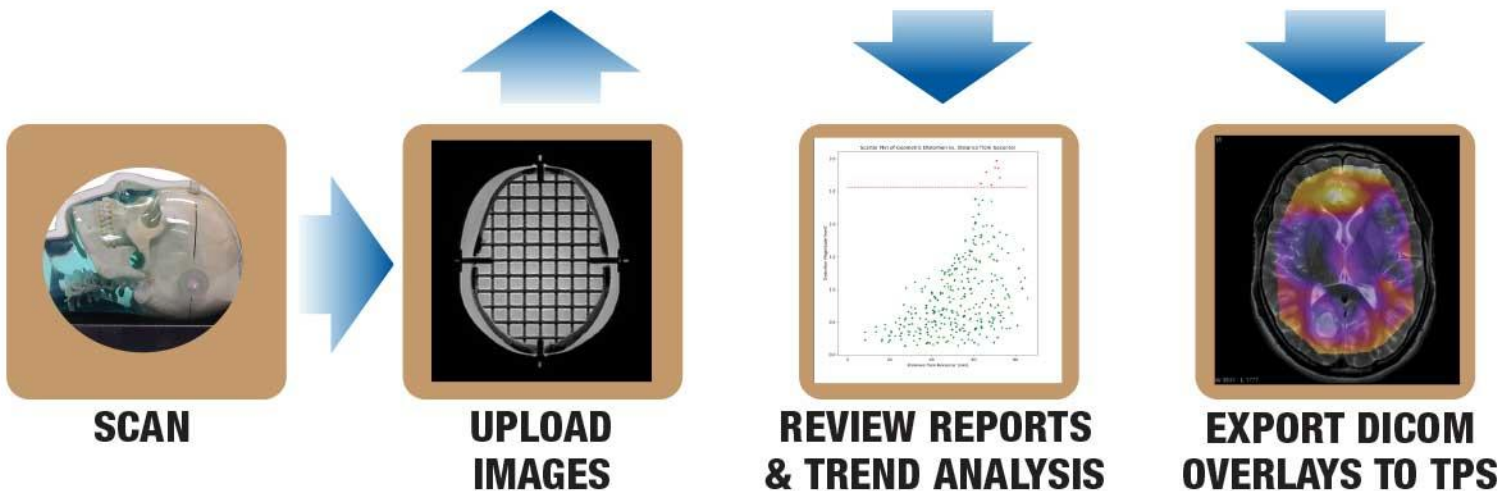
- CIRS proprietary materials simulate distortion due to susceptibility & chemical shifts typical to clinical patient scans

  - Density of physical control points optimized to bring interpolation close to linearity

  - Cloud based solution frees user of operating system and hardware constraints

  - Quickly & automatically analyze complete MR data sets

  - Online deployment facilitates collaboration, easy review and portability of results

Large Field Grid Phantom
2623 Physical Control Points

Visit us at ECR, Booth 128!

Inter-cranial Grid Phantom
335 Physical Control Points

CIRS

Microwave-induced thermoacoustic tomography through an adult human skull

An Yan
School of Electronics and Information Engineering, Sichuan University, Chengdu 610064, China
Caltech Optical Imaging Laboratory, Andrew and Peggy Cherng, Department of Medical Engineering, Department of Electrical Engineering, California Institute of Technology, Pasadena, CA 91125, USA

Li Lin
Caltech Optical Imaging Laboratory, Andrew and Peggy Cherng, Department of Medical Engineering, Department of Electrical Engineering, California Institute of Technology, Pasadena, CA 91125, USA
Department of Biomedical Engineering, Washington University in St. Louis, One Brookings Drive, St. Louis, MI 63130, USA

Changjun Liu[a)]
School of Electronics and Information Engineering, Sichuan University, Chengdu 610064, China

Junhui Shi, Shuai Na, and Lihong V. Wang[a)]
Caltech Optical Imaging Laboratory, Andrew and Peggy Cherng, Department of Medical Engineering, Department of Electrical Engineering, California Institute of Technology, Pasadena, CA 91125, USA

Purpose: To demonstrate the feasibility of microwave-induced thermoacoustic tomography (TAT) of adult human brain.

Methods: We analyzed the electric field distribution radiated from an antenna to acquire homogeneous illumination. We first imaged the anatomical structures in a rat's trunk to validate the thermoacoustic contrast *in vivo*. We then imaged an agar cylinder through an adult human skull *ex vivo* to demonstrate transcranial penetration of both microwave and ultrasound. We also analyzed the specific absorption rate to show the conformance to the safety standard for human electromagnetic exposure.

Results: We successfully acquired cross-sectional images of the rat's trunk *in vivo*. Major blood vessels and organs are clearly visible. The transcranial image shows that TAT can image through the adult human skull and reveal an agar enclosed by the skull.

Conclusions: Microwave-induced TAT of a rat's trunk *in vivo* and an agar phantom through an adult human skull *ex vivo* has been demonstrated experimentally. This study demonstrates both the TAT contrasts *in vivo* and the capability of transcranial imaging, showing potential of TAT for adult human brain imaging with high contrast and penetration. © *2019 American Association of Physicists in Medicine* [https://doi.org/10.1002/mp.13439]

Key words: adult human brain, microwave-induced thermoacoustic tomography, specific absorption rate (SAR), transcranial imaging

1. INTRODUCTION

It has been demonstrated that any significant cerebral dysfunction or disease, such as stroke and tumor, could lead to permanent neurological damage or death,[1] and many clinical trials have demonstrated the importance of early detection of brain stroke and tumors in improving survival.[2,3] Current high-resolution human brain imaging modalities include magnetic resonance imaging (MRI) and X-ray computed tomography (CT). MRI is costly, slow, and inapplicable to patients with claustrophobia.[4] X-ray CT utilizes ionizing radiation, and it is thus unsuitable for patients requiring frequent assessment.[5] Photoacoustic tomography (PAT) is a nonionizing imaging modality. However, the strong scattering of light limits the imaging depth within the brain.[6] In comparison, microwaves at appropriate frequencies penetrate tissue deeply, and thus microwave-induced thermoacoustic tomography (TAT) can potentially provide an effective tool for brain imaging. The various modalities are compared in Table I.

In TAT, biological tissues absorb pulsed electromagnetic energy and subsequently emit acoustic waves through thermal expansion.[7–10] The acoustic waves are then received by ultrasonic transducers and used to reconstruct the distribution of microwave absorption in the tissue.[11] The wide range of dielectric properties, related to physiological and pathological status, can lead to a high imaging contrast.[12,13]

Several transcranial TAT systems have been developed[14–16] and have advanced TAT toward clinical application, while ongoing limitations remain to be addressed. Most TAT transcranial studies used monkey skulls,[14,15] which are much thinner than the adult human skull. One group has demonstrated human-skull transcranial TAT *ex vivo* without validating the soft tissue contrast.[16] They did not analyze the specific absorption rate (SAR) to show the conformance to the safety standard for electromagnetic exposure. Due to the problematic

TABLE I. Comparison of imaging methods.

	MRI	X-ray CT	PAT	TAT
Resolution	Moderate	High	High	Moderate
Depth	Deep	Deep	Moderate	Deep
Cost	High	High	Low	Low
Portability	No	No	Yes	Yes
Acquisition time	Long	Short	Short	Short
Ionizing radiation	No	Yes	No	No

PAT, photoacoustic tomography; TAT, thermoacoustic tomography.

antenna placement in their experiment setup, the microwave reflected at the tank base would also illuminate the phantom without passing the skull. Here, we report an advancement in transcranial TAT technology that overcomes the aforementioned limitations. Our study demonstrates both soft tissue contrast *in vivo* and human-skull transcranial TAT, which produces an SAR lower than the safety limit.

2. MATERIALS AND METHODS

To study the TAT contrast of soft tissue *in vivo*, we first imaged a live rat. A schematic of the experimental setup is shown in Fig. 1(a). The rat was half-immersed in mineral oil. The microwave source had a peak power of 60 kW at 3 GHz and emitted 1.2-μs microwave pulses at a 10-Hz repetition rate. We used a custom-made horn antenna (WR284 horn antenna W/EEV flange, HNL Inc.) to illuminate the rat. It was found that a uniform distribution of the electric field could be acquired within a plane 4.5 cm above the horn

antenna [Fig. 1(c)]. An ultrasonic transducer (2.25-MHz central frequency, 0.5-inch diameter) was mounted on a rotary scanner. The thermoacoustic signals were first amplified by a two-stage low-noise amplifier and then transmitted to a data acquisition (DAQ) card set to a sampling frequency of 20 MHz. To image cross sections of the rat, we scanned the transducer circularly around the rat's trunk with 720 steps (0.5° step angle) and averaged signals 20 times at each scanning step. A half-time reconstruction algorithm was applied to mitigate image artifacts due to heterogeneous acoustic properties.[17] We then sacrificed the rat and photographed its abdominal cross section after imaging. All experimental animal procedures followed the laboratory animal protocol approved by the Animal Studies Committee of Washington University in St. Louis.

To eliminate microwave interference, we shielded the ultrasonic transducer surface with a metal mesh [Fig. 1(d)]. The dimension of the mesh holes was smaller than the microwave wavelength but larger than the ultrasonic wavelength. After showing the TAT contrast of the soft tissue *in vivo*, we further demonstrated the penetration of the microwave and ultrasound through an adult human skull *ex vivo*.

Because of the near-field illumination of microwave, an analysis of the SAR inside a head model is necessary to confirm the conformance to the safety standard for electromagnetic exposure. SAR measures the rate at which energy is absorbed by biological tissues when exposed to radio frequency electromagnetic fields. SAR is calculated as $\text{SAR} = \sigma E^2/2\rho$,[18] where σ is the electric conductivity (S/m), ρ is the mass density (kg/m^3), and E is the electric field (V/m). We developed a model of the human head illuminated by the
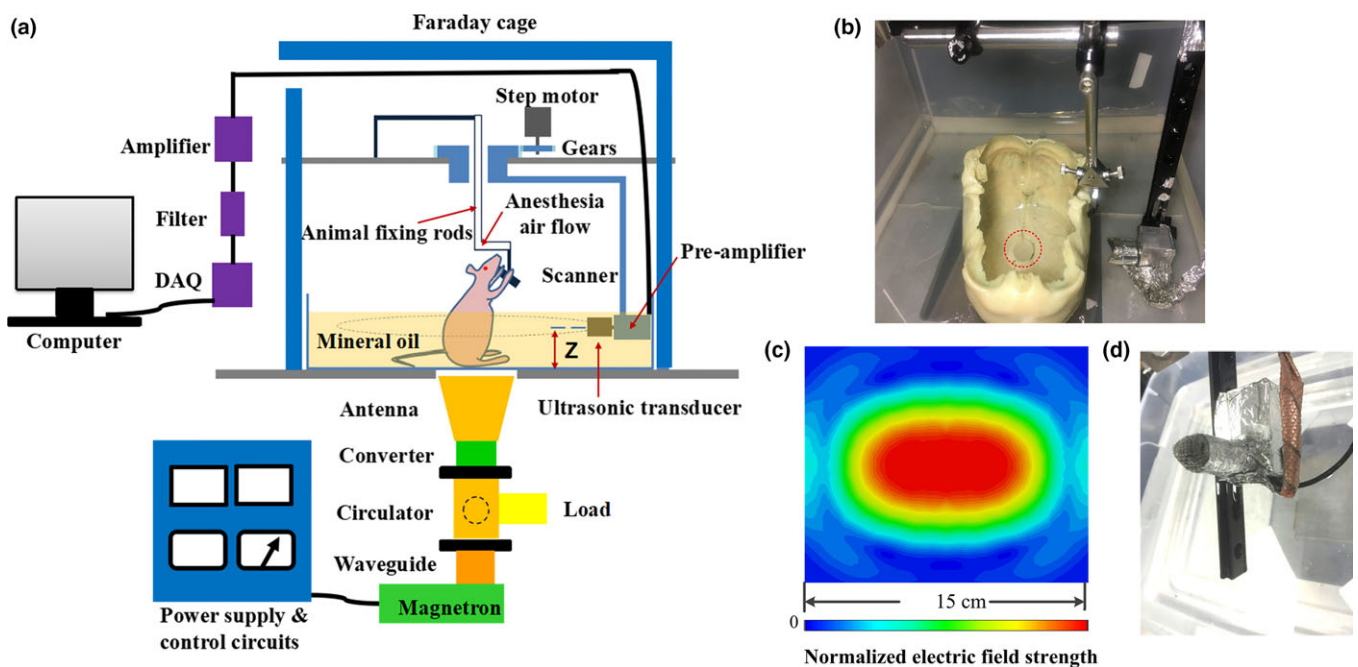

FIG. 1. (a) Schematic of the experimental TAT system. DAQ, data acquisition system. (b) Photograph of an agar cylinder (indicated by the red circle) placed inside an adult human skull. (c) Simulated electric field distribution in a plane 4.5 cm above the antenna. (d) Photograph of the ultrasonic transducer shielded with metal mesh.

antenna. The model had a skull with an 8-mm thickness. We assigned the relative permittivity, conductivity, and mass density of the skull to 3.7, 0.0016 S/m, and 1000 kg/m^3, respectively. We set the relative permittivity and conductivity of the brain to 50 and 2.48 S/m, respectively.[19] To simulate a scenario of the maximal microwave exposure in our system, we positioned the head model 1 cm away from the antenna [Fig. 2(a)]. Figure 2(b) shows the SAR distribution with a peak amplitude of 4×10^{-2} W/kg, which is far below the safety limit of the average SAR (2 W/kg) per IEEE EM safety standard (C95.1-2005).[18]

The geometry of the simplified skull transmission model is presented in Fig. 3(a). The acoustic shear waves in the skull is negligible when the incident angle is less than 20°.[20] If the skull is simplified as a hemisphere [Fig. 3(b)], the incident angle of the acoustic wave from the cortex on the skull's inner surface could be great than 20°. As a result, the shear wave component should not be overlooked. However, due to the high attenuation of shear wave in the oil, only a small portion of the shear wave can be transmitted to the transducer. Therefore, we considered the longitudinal wave only for image reconstruction.

Transcranial TAT was performed experimentally using an agar cylinder enclosed within an *ex vivo* human skull. The intact human skull was donated by an 83-year-old Caucasian male. The skull was fixed with a metal claw and before each experiment cleaned using hydrogen peroxide and a degreaser. The length, width, and height of the skull were 22, 15, and 15 cm, respectively. The thickness of the skull was inhomogeneous, ranging from ~ 7 mm (temporal area) to ~ 11 mm (frontal area). Figure 1(b) shows a photograph of the experimental setup. The agar cylinder was a homogenous dielectric cylinder with a 10 mm diameter and a 50 mm length. The microwave illuminates the skull from the bottom and the tank is housed with microwave absorbing foams. We also covered the skull opening with an agar pad to isolate the reflected microwave.

3. RESULTS

After shielding the transducer surface with metal mesh, the artifacts induced by microwave interference are significantly reduced (Fig. 4). The cross-sectional TAT image of the rat's trunk agrees well with the corresponding photograph [Fig. 5(a)]. The major vessels, spinal cord, and intestines are clearly revealed by TAT. Images of other cross sections (Z = 4, 5.5, and 7 cm) are shown in Fig. 5(b), where Z is the distance above the bottom of the tank.

The transcranial acoustic signals we received had a center frequency of 0.8 MHz [Fig. 6(a)]. An ultrasonic transducer (1-MHz center frequency, 1-inch diameter) was used to detect the thermoacoustic signals. We scanned the transducer circularly around the skull with 600 steps and averaged the signals 250 times at each scanning step. To compensate for the acoustic attenuation in the skull, we averaged more at each scanning step for a satisfactory signal-to-noise ratio. The TAT image clearly revealed the agar enclosed by the skull [Fig. 6(b)]. Applying an ultrasonic array would dramatically reduce the imaging time.
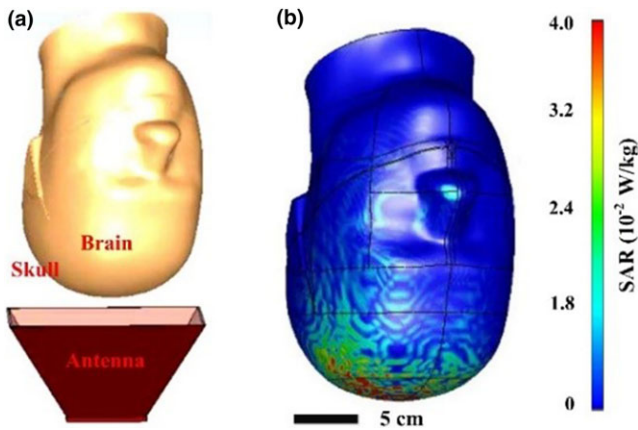

FIG. 2. (a) Simulation model of a head orienting toward the horn antenna. (b) SAR distribution with a peak SAR amplitude of 4×10^{-2} W/kg.
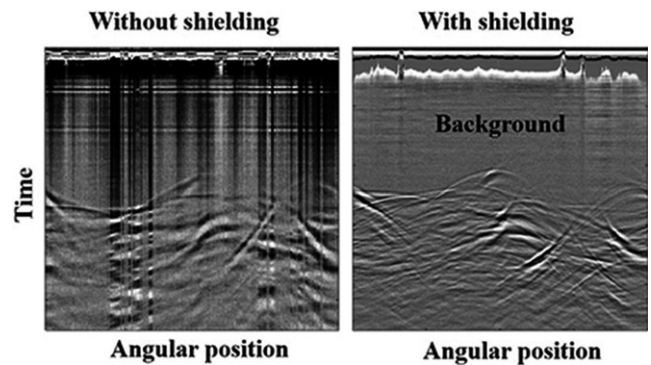

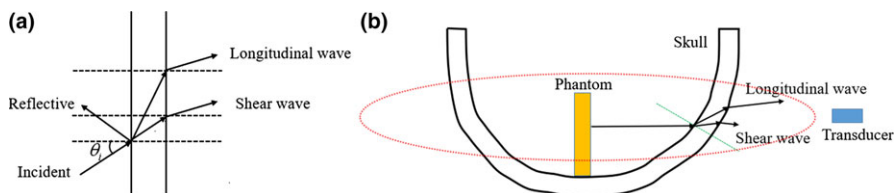FIG. 4. Diagrams of TAT signals acquired before and after shielding.

FIG. 3. (a) Planar model of ultrasonic propagation through the skull. (b) Hemispherical model of ultrasonic propagation through the skull.
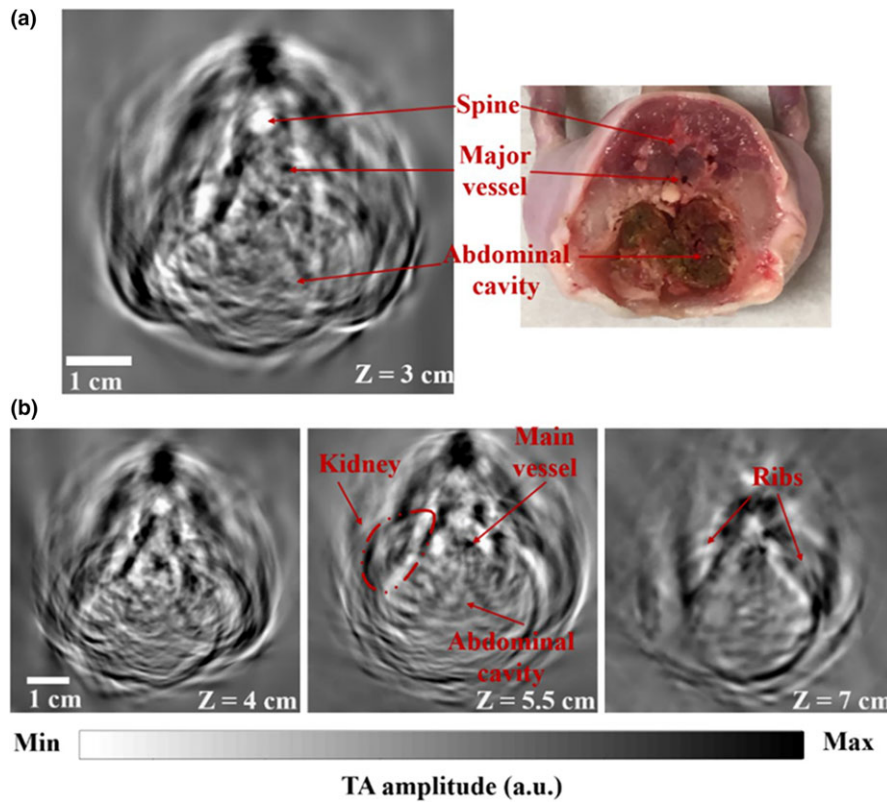
FIG. 5. Cross-sectional images of the rat's trunk. (a) TAT image and the corresponding photograph. (b) TAT images of the rat's trunk at different cross sections.
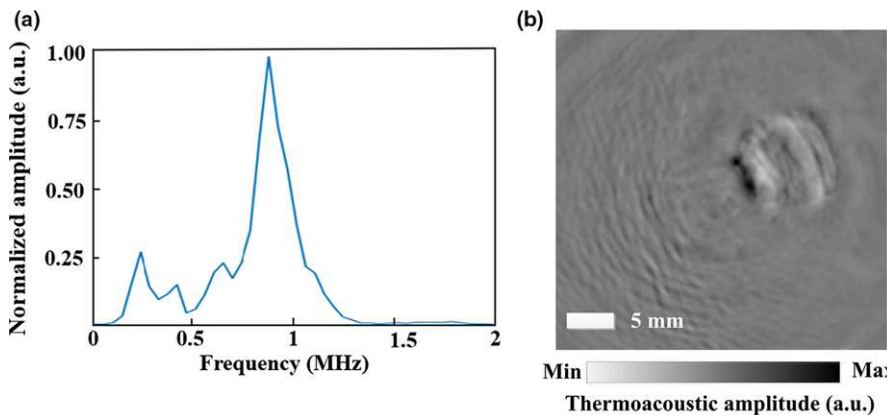

FIG. 6. Transcranial TAT. (a) Normalized spectrum of the transcranial TAT signal. (b) Transcranial TAT image of the agar.

4. DISSCUSIONS AND CONCLUSIONS

To demonstrate TAT for human brain imaging, we first used TAT to acquire cross-sectional soft tissue images of a rat's trunk *in vivo* to demonstrate the capability of imaging dielectric properties in soft tissues. The influence of the field distribution cannot be ignored when the object is larger than the microwave wavelength. Homogenous electric field distributions are preferred to reconstruct the microwave absorption coefficients. To examine the homogeneity, we analyzed the electric field distribution of the horn antenna. We also analyzed the SAR to demonstrate that the SAR was below the safety limit of the electromagnetic exposure to humans. From the spectrum of the thermoacoustic signal, we conclude that the transcranial acoustic signals had a center frequency of 0.8 MHz. We then demonstrated that microwave and 0.8 MHz ultrasound could penetrate an *ex vivo* adult human skull. Because of the difference in dielectric properties between hemorrhages or tumors and normal brain tissues,[21] microwave-induced TAT holds potential for detecting brain stroke and tumors.

There are both opportunities and challenges when TAT is applied to human brain imaging. To improve the imaging speed, an ultrasonic array with a multichannel DAQ system would be required. In addition, the instruments need to be carefully shielded. Because microwave has a much longer wavelength than the laser light, the system design is critical to achieving a uniform distribution of electric field. Algorithms that can compensate for the acoustic distortion induced by the skull would be helpful to improve the image quality.

In summary, TAT is a noninvasive and nonionizing imaging modality that can differentiate biological tissues with different dielectric properties. The one-way transcranial transmission of microwave and ultrasound enabled TAT for human brain imaging *ex vivo*. TAT, therefore, has the potential for detecting brain stroke and tumors *in vivo*.

ACKNOWLEDGMENTS

CONFLICT OF INTEREST

The authors have no conflicts to disclose.

[a] Authors to whom correspondence should be addressed. Electronic mails: cjliu@scu.edu.cn and LVW@caltech.edu.

REFERENCES

1. McKinney P. "Brain tumours: incidence, survival, and aetiology", journal of Neurology. *Neurosurg Psychiatry*. 2014;75:12–17.
2. Cha S. Update on brain tumor imaging: from anatomy to physiology. *Am J Neuroradiol*. 2006;27:475–487.
3. Castillo M. History and evolution of brain tumor imaging: insights through radiology. *Radiology*. 2014;273:111–125.
4. Ellegood J, Babineau BA, Henkelman RM, Lerch JP, Crawley JN. Neuroanatomical analysis of the BTBR mouse model of autism using magnetic resonance imaging and diffusion tensor imaging. *Neuro Image*. 2013;70:288–300.
5. Collingwood J, Adams F. Chemical imaging analysis of the brain with X-ray methods Spectrochim. *Nat Methods*. 2011;8:662–664.
6. Nie L, Cai X, Maslov K, Garcia-Uribe A, Anastasio MA, Wang LV. Photoacoustic tomography through a whole adult human skull with a photon recycler. *J Biomed Optics*. 2012;17:110506.
7. Wang LV, Zhao X, Sun H, Ku G. Microwave-induced acoustic imaging of biological tissues. *Rev Sci Instrum*. 1999;70:3744–3748.
8. Gao F, Zheng Y, Feng X. Magnetically mediated thermoacoustic imaging toward deeper penetration. *Appl Phys Lett*, 2013;103: 093704.
9. Gao F, Zheng Q, Zheng Y. Electrical circuit modeling and analysis of microwave acoustic interaction with biological tissues. *Med Phys*. 2014;41:053302.
10. Yan A, Lin L, Na S, Liu C, Wang LV. Large field homogeneous illumination in microwave-induced thermoacoustic tomography based on a quasi-conical spiral antenna. *Appl Phys Lett*. 2018;41: 123701.
11. Wang X, Qin T, Witte RS, Xin H. Computational feasibility study of contrast-enhanced thermoacoustic imaging for breast cancer detection using realistic numerical breast phantoms. *IEEE Trans Microw Theory Tech*. 2015;63:1489–1501.
12. Ding W, Ji Z, Xing D. Microwave-excited ultrasound and thermoacoustic dual imaging. *Appl Phys Lett*. 2017;110:183701.
13. Gao F, Feng X, Zheng Y. Advanced photoacoustic and thermoacoustic sensing and imaging beyond pulsed absorption contrast. *J Opt (United Kingdom)*. 2016;18:18–25.
14. Xu MH, Wang LHV. Time-domain reconstruction for thermoacoustic tomography in a spherical geometry. *IEEE Trans Med Imaging*. 2002;21:814–822.
15. Xu Y, Wang LV. Rhesus monkey brain imaging through intact skull with thermoacoustic tomography. *IEEE Trans Ultrason Ferroelectr Freq Control*. 2006;53:542–548.
16. Huang L, Li T, Jiang H. Technical Note: thermoacoustic imaging of hemorrhagic stroke: a feasibility study with a human skull. *Med Phys*. 2017;44:1494–1499.
17. Jin X, Li CH, Wang LV. Effects of acoustic heterogeneities on transcranial brain imaging with microwave-induced thermoacoustic tomography. *Med Phys*. 2008;35:3205–3214.
18. IEEE Standard for Safety Levels with Respect to Human Exposure to Radio Frequency Electromagnetic Fields 3 kHz to 300 GHz," IEEE Std C95.1-2005 (Revision of IEEE Std C95.1-1991), 2006.
19. Gabriel S, Lau R, Gabriel C. The dielectric properties of biological tissues: II. Measurements in the frequency range 10 Hz to 20 GHz. *Phys Med Biol*. 1996;41:2251–2269.
20. White PJ, Clement GT, Hynynen K. Longitudinal and shear mode ultrasound propagation in human skull bone. *Ultrasound Med Biol*. 2006;32:1085–1096.
21. Ku G, Wang LV. Scanning microwave-induced thermoacoustic tomography: signal, resolution, and contrast. *Med Phys*. 2001;28:4–10.